https://doi.org/10.5194/egusphere-2026-561
Preprint. Discussion started: 4 February 2026

UAV-based method for measuring CO_2 emissions in forest ecosystems

Haijiong Sun[1], Shao-Meng Li[1*], Yifei Wang[3], Yanrong Yang[4], Tianran Han[5], Keyu Chen[1], Chang Liu[1], Jietao, Zhou[1], Zeqing Ma[2], Fengting Yang[2], Junfei Guo[6], Xiangyu Gao[6]

[1] College of Environmental Sciences and Engineering, Peking University, Beijing 100871, China

[2] Qianyanzhou Ecological Research Station, Key Laboratory of Ecosystem Network Observation and Modeling, Institute of Geographic Sciences and Natural Resources Research, Chinese Academy of Sciences, Beijing 100101, China

[3] Inner Mongolia Institute of Metrology and Testing, Hohhot 010060, China

Key Lab. for Restoration and Reconstruction of Degraded Ecosystems in Northwestern

[4] China of Ministry of Education, School of Ecology and Environment, Ningxia University, Yinchuan 750021, China

[5] China Electric Power Research Institute, Beijing 100192, China

[6] Beijing Wisdominc Technology Co., Ltd, Beijing 100070

* Correspondence to: Shao-Meng Li (shaomeng.li@pku.edu.cn)

https://doi.org/10.5194/egusphere-2026-561
Preprint. Discussion started: 4 February 2026

Abstract

This study addresses the difficulty of accurately quantifying CO_2 emissions in forest ecosystems due to spatial heterogeneity, complex terrain, and the combined effects of horizontal and vertical transport. A UAV-based platform, capable of three-dimensional CO_2 emission observation, was developed, evaluated and applied to a forest ecosystem. The system integrates a high-precision closed-path CO_2 analyzer with a calibrated ultrasonic anemometer, and employs complementary box-pattern and profile-pattern flight strategies within a mass-balance framework to simultaneously resolve horizontal transport and vertical exchange. Validation against a long-term eddy-covariance (EC) flux tower shows that vertical CO_2 fluxes derived using the gradient method agree well with EC observations across seasons ($R^2 \approx 0.76$–0.77). Box-pattern flights further reveal pronounced diurnal variation: lateral advection dominates in the early morning, whereas vertical uptake prevails under well-mixed midday conditions. Sensitivity analyses across scales of 50 m, 100 m, 150 m indicate that CO_2 emission intensity is sensitive to control-volume dimensions and shows spatial heterogeneity above the forest. Uncertainty assessment suggests that the total relative uncertainty of UAV-derived emissions is typically ~15%, with wind-field calibration as the main error source. Overall, this UAV approach provides a flexible and reliable complement for analyzing near-surface three-dimensional CO_2 transport over complex and heterogeneous forests, helping to overcome the limited spatial coverage of traditional flux towers and remote sensing.

Keywords: UAV-based observations; CO_2 emissions; Mass balance; Three-dimensional flux measurement; Spatial heterogeneity

https://doi.org/10.5194/egusphere-2026-561
Preprint. Discussion started: 4 February 2026

1 Introduction

Carbon dioxide (CO_2) is the dominant anthropogenic greenhouse gas in the atmosphere, contributing approximately 50–60% to the enhanced greenhouse effect excluding water vapor (WMO, 2023). Atmospheric CO_2 budget, however, is strongly impacted by biospheric carbon cycles. Forest ecosystems, in particular, play a critical role in the terrestrial carbon cycle and are widely recognized as major carbon sinks, covering about 40% of the global land surface and representing some of the most extensive and structurally complex ecosystems on Earth (Bonan, 2008; IPCC, 2021; Pan et al., 2011). Consequently, an accurate understanding of carbon exchange processes between forests and the atmosphere is essential for assessing regional and global carbon budgets and their feedbacks on climate change. However, despite decades of carbon-cycle research to estimate CO_2 exchange across spatial scales, including eddy covariance (EC) towers, satellite-based remote sensing, and manned aircraft measurements (Baldocchi, 2003; Gioli et al., 2004; Jung et al., 2020), most existing methods are inherently confined to either vertical or horizontal dimensions due to theoretical or practical limitations, which restrict their ability to represent the full three-dimensional structure of CO_2 transport in the lower atmosphere (Leuning et al., 2008). In forest ecosystems, strong spatial heterogeneity, complex canopy–atmosphere interactions, and non-negligible horizontal transport processes can introduce substantial uncertainties into quantitative estimates of ecosystem–atmosphere CO_2 exchange (Baldocchi, 2008; Schimel et al., 2015). As a result, approaches capable of resolving both horizontal and vertical CO_2 transport are required.

Eddy covariance (EC) flux measurement technique is currently the most widely used method for quantifying ecosystem-scale vertical CO_2 fluxes and has been implemented globally through networks such as the FLUXNET (Aubinet et al., 2012; Baldocchi et al., 2001; Baldocchi, 2003; Wilson et al., 2002). By design, EC provides direct measurements of time-averaged vertical turbulent flux of CO_2 between the surface and the atmosphere. However, the method relies on the validity of the Monin–Obukhov Similarity Theory (MOST), which assumes a horizontally homogeneous, flat

https://doi.org/10.5194/egusphere-2026-561
Preprint. Discussion started: 4 February 2026

terrain and stationary turbulence (Foken, 2008; Kaimal and Finnigan, 1994; Monin and Obukhov, 1954; Stull, 1988). Over forested or topographically complex terrains, these assumptions are often violated, calling into question the representativeness of EC flux measurement results over such ecosystems. EC flux measurements do not explicitly resolve horizontal CO_2 transport associated with advection, canopy heterogeneity, terrain-induced flows, or mesoscale circulations (Aubinet et al., 2002; Feigenwinter et al., 2004; Finnigan et al., 2003; Leuning et al., 2005). Horizontal fluxes are therefore commonly neglected or assumed to be negligible in EC flux measurements, an assumption that may not hold under weak or non-stationary turbulence conditions (Mahrt, 1998, 2010; Vickers and Mahrt, 1997). In addition, EC towers provide flux information at a fixed height, limiting their ability to characterize CO_2 transport at different levels within the atmospheric boundary layer (Schmid, 2002), hence unable to determine flux divergence. For large scale atmosphere-ecosystem CO_2 exchanges, satellite remote sensing offers valuable information on horizontal distributions of atmospheric pollutants (Crisp et al., 2017; Jacob et al., 2016), but it has limited sensitivity to vertical gradients near the surface and cannot resolve canopy-scale exchange processes with the accuracy of in situ measurements (Chevallier et al., 2014). Likewise, manned aircraft campaigns provide regional-scale observations of pollutants distributions and enable mass-balance approaches to emission estimation (Cambaliza et al., 2014), but vertical fluxes are difficult to determine (Gordon et al., 2015). Collectively, these limitations highlight a persistent observational gap in the characterization of CO_2 three-dimensional transport in forest ecosystems.

Recent advances in rotating wing unmanned aerial vehicle (UAV) platforms and lightweight sensor technologies have created new opportunities for atmospheric measurements over complex environments. UAVs have emerged as practical tools for complementing existing carbon observation networks by enabling flexible, high-resolution measurements of greenhouse gases in both horizontal and vertical directions (Bolek et al., 2024; Khan et al., 2012; Villa et al., 2016). Compared with fixed EC towers, UAVs can directly measure concentration spatial variability over short time and

https://doi.org/10.5194/egusphere-2026-561
Preprint. Discussion started: 4 February 2026

spatial scales without relying on assumptions of horizontal homogeneity (Witte et al., 2017), enabling identification of emission or uptake hotspots that may be missed by ground-based observations (Khan et al., 2012). Nonetheless, these UAV applications have not demonstrated the feasibility of CO_2 flux measurements owing to their inability to conduct accurate wind speed and greenhouse gas concentration measurements, partially due to platform-induced airflow disturbances and rapidly changing flight attitude (Soltaninezhad et al., 2025; Thielicke et al., 2021). To address these challenges, various sensors, including multi-hole probes, pitot tubes, and sonic anemometers, have been deployed on UAVs for wind measurements and correction algorithms have been developed for disturbances (Langelaan et al., 2011; Niedzielski et al., 2017; Nolan et al., 2018; Rogers and Finn, 2013; Soddell et al., 2004; Spiess et al., 2007). Among these, sonic anemometers are considered particularly promising because of their high accuracy and fast response (Thielicke et al., 2021). Nevertheless, the influence of rotor-induced flow distortion, UAV attitude changes, and local turbulence on wind measurements remains non-negligible and requires dedicated calibration strategies (Soltaninezhad et al., 2025).

Building on our previous work on the development of an UAV platform for integrated high sensitivity, high precision, fast response measurements of GHG concentrations and 3-D wind speed, combined with a comprehensive wind calibration algorithm to correct for UAV motion, attitude, and rotor effects (Yang et al., 2025), we aim to improve quantification of atmospheric CO_2 transport in both horizontal and vertical directions over forest ecosystems. In the present study, we evaluate the UAV platform and the wind correction algorithm to assess its ability to determine three-dimensional CO_2 transport including canopy-scale vertical CO_2 fluxes, and to evaluate the robustness and uncertainty of the UAV-derived emission estimates. The evaluation is based on specifically designed flight strategies with complementary box and profile flight patterns and is conducted in field experiments at a subtropical forest site. Such flight strategies are implemented within a mass-balance framework to resolve three-dimensional CO_2 exchange in the lower atmosphere. While horizontal mass flux

https://doi.org/10.5194/egusphere-2026-561
Preprint. Discussion started: 4 February 2026

measurements using this platform have been previously evaluated and validated in field measurements (Han et al., 2024) vertical fluxes derived from such a platform have not been evaluated until now, and a critical part of the present study is to validate the UAV vertical flux measurement methodology against the collocated tower-based EC flux measurements. As presented further below, the results demonstrate a highly versatile methodology for determining net carbon fluxes out of complex ecosystem terrains that not only complements existing carbon flux tower measurements but also resolves underlying issues related to horizontal carbon transport not addressed in carbon cycle research previously.

2 Field site and platform description

2.1 Platform description

2.1.1 UAV platform

The UAV platform used in this study is a battery-powered hexacopter (KWT-X6L-15, ALLTECH, China), which provides stable flight performance and high maneuverability, including vertical take-off and landing, hovering, and controlled horizontal flight (Fig. 2b). This airframe was selected as the base platform for CO_2 measurements because of its ability to operate safely above forest canopies, its high payload capacity, and its adaptability to multiple flight strategies. The UAV has a maximum span of arm plus rotor blade of 2570 mm, and the height from the body stands to the body top is 565 mm. Its maximum horizontal flight speed is 18 m s^{-1}, the maximum ascending rate is 4 m s^{-1}, and the maximum wind resistance is 14.4 m s^{-1}, all of which satisfy the requirements for atmospheric wind and CO_2 measurements in the lower boundary layer. A detailed summary of the UAV specifications is provided in Table 1.

Table 1. Specifications and capabilities of the UAV.

hover endurance	≥30 min (for 15 kg payload)
Peak flight velocity	18 m s^{-1}
Peak climb velocity	4 m s^{-1}

https://doi.org/10.5194/egusphere-2026-561
Preprint. Discussion started: 4 February 2026

Control radio range	≥7 km
Operating ambient temperature	-20 ℃~55 ℃
Maximum operating altitude	≥5000 m
Wind resistance capability	14.4 m s^{-1}
Payload capacity	15 kg (without battery)
Rotor blade length	765±5 mm
Symmetric motor center-to-center length	1635±10 mm
Body stands to the body top length	565 ± 5 mm
Wing span	2570 ±10 mm
Battery capacity/unit	30000 mAh (2 units)
Battery weight/unit	6 kg ± 0.1 kg
Radio modem	902 MHz ~928 MHz
GPS accuracy	Horizontal direction: ± (8+10^{-6}D) mm; Vertical direction: ± (15+10^{-6}D) mm
Navigation	GPS (RTK system)

The airframe is constructed from carbon-fiber composite materials and houses an integrated flight control system, a power supply module, and a communication unit. The flight control system includes an inertial measurement unit (IMU), accelerometers, and a global positioning system (GPS) capable of real-time kinematics (RTK), and records UAV attitude and motion parameters (roll, pitch, yaw, and three-axis accelerations) which is critical for subsequent wind-speed correction. To improve positioning accuracy, the onboard RTK GPS receiver takes in real-time signals from a concurrently ground-deployed kinematic (RTK) GPS system (iRTK10, Hi-Target, China) for real time computation for centimetre- to millimetre-level accuracies in both the horizontal and vertical directions, which are particularly advantageous over a complex terrain. The power module consists of two lithium–polymer batteries connected in parallel, each with a capacity of 30,000 mAh, enabling a maximum payload of 15 kg and a typical flight endurance of approximately 30 min. The communication module operates in the 890-960 MHz frequency band, allowing reliable telemetry and control within a range of up to 10 km.

2.1.2 Scientific payloads

The integrated scientific payloads, with a total weight of 6.35 kg including the mounting chassis, were powered directly by the main UAV batteries. The payloads include a closed-path CO_2 analyzer and a 3-d ultrasonic anemometer, with their

https://doi.org/10.5194/egusphere-2026-561
Preprint. Discussion started: 4 February 2026

specifications summarized in Table 2. The 3-d ultrasonic anemometer (Trisonica Mini, LI-COR Environment, USA) is a compact sensor, with a measurement path of 35 mm and a mass < 50 g, that measures three-dimensional wind speeds under its own coordinate system, air temperature, and pressure. The anemometer was mounted 70 cm above the rotor plane to minimize flow distortion caused by propeller blade downwash (Fig. 1b) (Yang et al., 2025). This configuration has been shown to achieve acceptable accuracy (±2 %) in previous validation studies using reference-grade meteorological instruments (Palomaki et al., 2017; Shimura et al., 2018; Thielicke et al., 2021). The CO_2 analyzer (MIRA Ultra N_2O/ CO_2, Aeris Technologies, USA) was mounted beneath the UAV body to measure CO_2 volume mixing ratios in air, with its air inlet set next to the anemometer sonic sensors to ensure spatially consistent wind and CO_2 concentration measurements. A fixed time lag of 5 s, associated with air residence time in the sampling line, was applied to synchronize the CO_2 measurements with the wind data.

Data from all scientific payloads, together with UAV attitude and flight parameters (roll, pitch, yaw, three-axis accelerations, and GPS position), were recorded by the onboard main controller via UART communication and stored on an SD card (Fig. 1). In addition, real-time telemetry, including sensor status, battery voltage, and flight parameters, was transmitted to a ground station, allowing continuous monitoring during flight operations. The CO_2 measurements were recorded at 1 Hz, while the anemometer data were recorded at 5 Hz.

Table 2. Detailed information of scientific payloads.

Instrument	Sample Frequency (Hz)	Weight (kg)	Measurement	Accuracy
MIRA Ultra	1	6	CO_2	< 200 ppb/s
Trisonica Mini	5	0.05	Wind speed	(0 - 10 m/s): ±0.2 m/s
				(11 - 30 m/s): ±2%
			Wind direction	± 1.0°
			T	± 2.0 °C
			P	± 1.0 kPa

https://doi.org/10.5194/egusphere-2026-561
Preprint. Discussion started: 4 February 2026

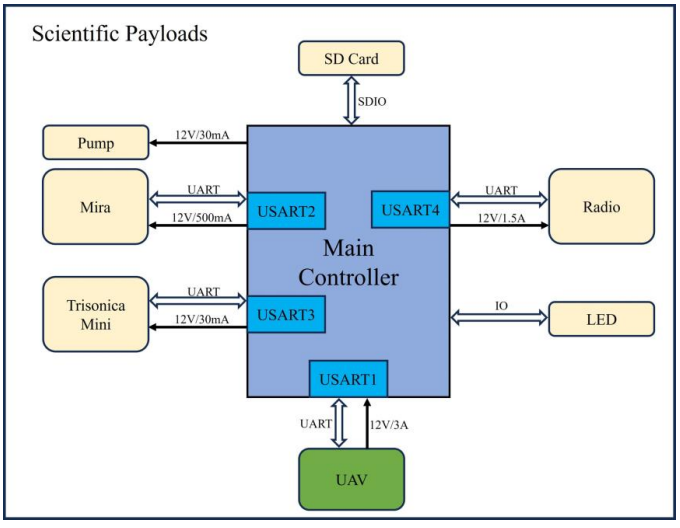

Figure 1. Diagram of the scientific payloads on the UAV-based flux measurement system.

2.2 Field site description

The UAV-based field measurements were conducted at the Qianyanzhou Experimental Station (26°44′29″ N, 115°03′29″ E) located in Jiangxi Province, southern China. This station is one of the core flux observation sites of the China Flux Observation Research Network (ChinaFLUX) and is equipped with a comprehensive eddy covariance (EC) measurement system (Yu et al., 2006). The EC tower has a height of approximately 43 m above ground, with the EC system installed at 31 m above ground level, while the mean forest canopy height is about 18 m.

The long-term observation site, 1 ha in size and centred on the EC tower, is dominated by plantation forests, primarily consisting of *Pinus massoniana*, *Cunninghamia lanceolata*, and *Pinus elliottii* arranged in a strip-mixed pattern with an approximate ratio of 49:48:3, respectively (Huang et al., 2007). The region experiences a typical subtropical monsoon climate, characterized by prevailing southerly winds in summer and northerly winds in winter. The mean annual air temperature is 17.9 °C, and the mean annual precipitation is approximately 1490 mm, with most rainfall occurring between March and June.

https://doi.org/10.5194/egusphere-2026-561
Preprint. Discussion started: 4 February 2026

To evaluate the performance of the UAV platform for CO_2 vertical flux measurements, measurement flights were conducted at Site B, located approximately 160 m southeast of the EC tower (Site A), and direct comparisons with tower-based measurements were performed (Fig. 2a). Based on a comprehensive site survey, Site B was selected as the UAV take-off and landing location because of its relatively open forest structure, complex surrounding vegetation, and a lower elevation (~15 m lower) than Site A, which facilitates safe UAV operations. Within a radius of approximately 350 m northwest of Site B, only a limited number of low-rise buildings below the forest canopy used exclusively for scientific research are present, resulting in minimal anthropogenic influence on the measured CO_2 fluxes. Such an experimental condition provides a representative forest ecosystem setting in which UAV-derived fluxes can be evaluated against EC tower observations.

From May 2023 to December 2024, a total of 209 UAV flights were conducted at the site, corresponding to approximately 100 h of cumulative flight time. After data quality controls, including the removal of records affected by rainfall and other conditions that could compromise instrument performance, results from 168 flights were retained for analysis, including 40 flights in spring, 55 in summer, 53 in autumn, and 20 in winter.

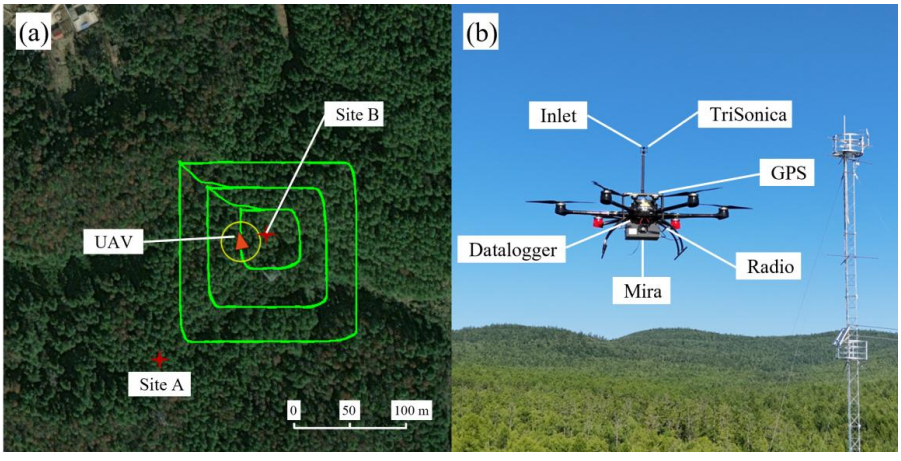

Figure 2. (a) A top-down view of the UAV's flight tracks. The green flight tracks represent the box

https://doi.org/10.5194/egusphere-2026-561
Preprint. Discussion started: 4 February 2026

pattern, categorized into three box sizes: 50×50 m, 100×100 m, and 150×150 m. Site A marks the location of the flux tower where EC measurements of vertical CO_2 fluxes are continuously carried out, while Site B denotes the take-off point for the profile pattern. The straight-line distance between the two sites is 150 m. (b) The instrumented UAV platform; the flux tower can be seen in the background.

2.3 Flight patterns

Two complementary flight strategies were executed in this study: a box pattern and a profile pattern (Fig. 3a). The box pattern consists of a closed rectangular flight path flown above the forest canopy at multiple altitudes, enabling sampling of horizontal CO_2 transport across a defined control volume. Box flights were conducted at heights of 35, 40, 45, 50, 60, 80, and 100 m above ground level. Using flight-path fitting and screen interpolation (Han et al., 2024), the three-dimensional spatial distributions of CO_2 volume mixing ratio, wind vectors, and air density were reconstructed within the box domain (Fig. 3b). Flight-path fitting refers to the construction of a smooth, closed loop constructed from the discrete UAV trajectories at all altitudes, thereby defining the four virtual vertical surfaces of the box. Screen interpolation refers to the mapping of CO_2 mixing ratios and corrected wind speed measurements observed along the flight path onto a regular two-dimensional grid on the vertical surfaces, which enables numerical integration of fluxes across each box wall.

The profile pattern was designed to capture vertical gradients of CO_2 mixing ratios, wind speed, and air density from near the surface to the top measurement height. Each box-pattern flight was paired with a vertical profile, and all measurements were completed within approximately 20 min to ensure consistency of the sampled air mass in the controlled volume. Vertical CO_2 fluxes were computed from the profile data using the gradient method (Sect. 3.2.2), with the analysis height range defined by the lowest and highest box levels (35–100 m). Because the EC system is installed at 31 m, UAV-derived CO_2 vertical fluxes used data from 28 and 33 m to enable direct comparison with tower-based EC measurements.

https://doi.org/10.5194/egusphere-2026-561
Preprint. Discussion started: 4 February 2026

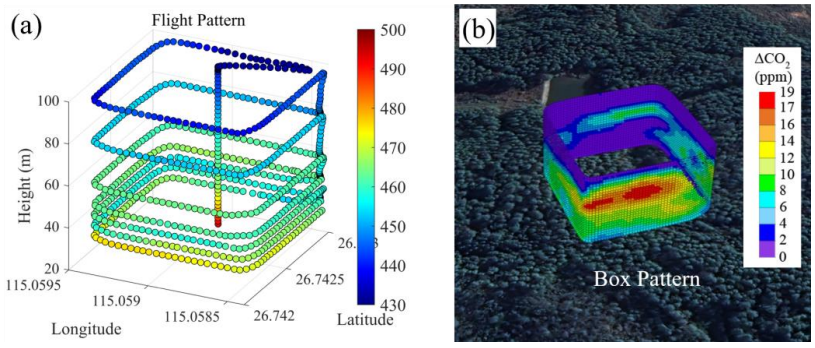

Figure 3. Overview of flight patterns. (a) Two distinct flight strategies: box pattern and the profile pattern. (b) The spatial distribution of CO_2 mixing ratios obtained through flight-path fitting and screen interpolation for flights during 2024-08-08 7:00 – 7:30, morning.

3 Methodologies

3.1 Wind speed calibration

To obtain accurate and reliable wind speed measurements, the raw data acquired by the ultrasonic anemometer were processed using a dedicated wind speed calibration algorithm. This algorithm, developed by Yang et al. (2025), employs computational fluid dynamics (CFD) simulations to characterize the flow-field distortion by the UAV rotor-induced airflows. Hundreds of simulation scenarios were conducted, encompassing a wide range of flight altitudes, wind directions, and ambient wind speeds, in order to quantify the influence of rotor-induced airflow disturbances on wind measurements. The simulated disturbance fields were subsequently combined with UAV motion and attitude compensation schemes, yielding a comprehensive correction algorithm that simultaneously accounts for UAV translation, rotation, and rotor effects. The algorithm was validated with 3-D wind measurements at multiple levels on an 80-meter met tower Yang et al. (2025). All wind measurements used in this study were corrected using this algorithm, ensuring consistency and comparability with reference-grade wind observations.

3.2 CO_2 emission estimation based on UAV measurements

CO_2 emissions from within the control volume defined by the virtual box were

https://doi.org/10.5194/egusphere-2026-561
Preprint. Discussion started: 4 February 2026

quantified using a mass-balance framework that integrates measurements obtained from box-pattern and profile-pattern UAV flights. This approach assumes that CO_2 emitted within the control volume is transported by the mean wind field and becomes sufficiently mixed, such that the net emission rate can be inferred from the fluxes crossing the boundaries of the volume. Under steady or quasi-steady wind conditions, the mass flux of a chemical compound through a plane perpendicular to the mean wind direction can be considered approximately constant.

According to the divergence theorem, the rate of change of mass of a stable compound within a control volume equals the surface integral of the mass flux through its enclosing surfaces. Consequently, the total CO_2 emission rate within the volume equals the net outward flux integrated across all box wall surfaces. Based on the integral form of the continuity equation, the emission rate within the control volume enclosed by the box pattern can be expressed as

$$E_C = E_{C,H} + E_{C,HT} + E_{C,V} + E_{C,VT} - E_{C,M} \quad (3.1)$$

where E_C denotes the total CO_2 emission rate within the control volume, $E_{C,H}$ and $E_{C,V}$ denote the integrals of horizontal and vertical advective fluxes through the box walls, respectively; $E_{C,HT}$ and $E_{C,VT}$ represent the integrated turbulent fluxes in the horizontal and vertical directions, and $E_{C,M}$ accounts for changes in CO_2 mass associated with air-density variations. Eq. (3.1) forms the basis of the TERRA emission inversion model (Gordon et al., 2015).

To investigate the contributions of each component to the emissions, the TERRA model was updated here, in particular the treatment of the vertical flux algorithm, to directly compute vertical turbulent fluxes based on the UAV measurements instead of relying on parametrization assuming entrainment. Here, the mean wind vectors ($\bar{u}$, $\bar{v}$, $\bar{w}$) measured with the UAV sonic anemometer over a 30-minute period and the corresponding wind fluctuations (u', v', w') are used to determine fluxes in the three directions. For the horizontal terms, the mean horizontal wind speed $\bar{u}$ can be regarded as the main contributor to the $E_{C,H}$ term, typically 2–3 m/s. The horizontal turbulent velocity (u') is the main contributor to $E_{C,HT}$. Using the 95th percentile of u', the turbulent velocity is less than 0.02 m/s. The horizontal advection term ($E_{C,H}$) is larger

https://doi.org/10.5194/egusphere-2026-561
Preprint. Discussion started: 4 February 2026

than the turbulence term ($E_{C,HT}$) by more than 100 times, so that the $E_{C,HT}$ term can be neglected from Eq. (3.1). For the vertical flux terms, the reverse is true; the mean vertical wind speed $\bar{w}$, at typically <0.02 m/s, makes $E_{C,V}$ a minute contribution compared to the turbulent flow contribution $E_{C,VT}$, which depends on the vertical turbulent velocity (w'). Using the 95th percentile of w', the turbulent velocity can reach 0.3 m/s. As such, vertical advection term can also be neglected from Eq. (3.1).

The density-related term can be expressed as

$$E_{C,M} = M_R \iiint \chi_C \frac{d\rho_{air}}{dt} dxdydz \quad (3.2)$$

Because the maximum vertical (≈65 m), horizontal (≈150 m) extents, and duration of the UAV flights are limited, air-density variation over time $\frac{d\rho_{air}}{dt}$ within the control volume can be assumed to be negligible, and $E_{C,M}$ was therefore neglected. Accurate estimation of the remaining flux terms ($E_{C,H}$ and $E_{C,VT}$) enables computation of the net CO_2 emission rate. The reliability of the box-pattern approach for resolving CO_2 emission is further supported by Han et al. (2024), who conducted a series of controlled UAV-based CO_2 validation experiments over an industrial coking facility.

3.2.1 Computation of CO_2 horizontal emission component

The horizontal emission component was derived from box-pattern measurements by integrating the advective CO_2 flux across the four vertical walls of the virtual box. The horizontal CO_2 emission rate can be written as

$$E_{C,H} = M_R \oiint \chi_C(s,z)\rho_{air}(s,z)U_{\perp}(s,z)dsdz \quad (3.3)$$

For each altitude level, the line flux $F(z)$ was first calculated from the box-pattern data as

$$F(z) = M_R \sum_0^L \left(\chi_C(s,z) \cdot \rho_{air}(s,z) \cdot u_{\perp}(s,z)\right) \cdot \Delta s \quad (3.4)$$

where Δs denotes the distance travelled during each 1 s sampling interval, and L represents the total length of the closed flight path at that altitude.

To suppress small-scale variability, a moving average was applied to consecutive line-flux values, yielding layer-averaged fluxes for discrete altitude intervals. These

https://doi.org/10.5194/egusphere-2026-561
Preprint. Discussion started: 4 February 2026

layer-integrated values were then vertically integrated to obtain the total horizontal CO_2 emission rate

$$E_{C,H} = \sum_0^N F(z) \cdot \Delta z = M_R \sum_0^N (\sum_0^L (\chi_C(s,z) \cdot \rho_{air}(s,z) \cdot u_n(s,z)) \cdot \Delta s) \cdot \Delta z \quad (3.5)$$

where Δz denotes altitude intervals and N denotes N sets of line flux values.

3.2.2 Computation of vertical emission component

The vertical CO_2 emission component was estimated from profile measurements using the gradient method, which relates turbulent scalar fluxes to vertical gradients of the scalar concentration. In practice, vertical profiling over forested terrain is operationally challenging, and UAV measurements were conducted at a single representative location. The resulting vertical fluxes were assumed to be representative of the broader domain, an assumption evaluated through direct comparison with eddy covariance (EC) tower measurements (see Section 4.2.1).

The vertical CO_2 emission component was obtained from integrating the vertical flux over the horizontal area enclosed by the box pattern and can be approximated by the product of vertical flux and the horizontal area, expressed as

$$E_{C,VT} = \iint F_v dx dy = A \cdot F_v \quad (3.6)$$

where F_v denotes the vertical flux and A is the horizontal area of the control volume.

According to the flux–gradient relationship, turbulent scalar fluxes are proportional to the vertical gradient of the scalar quantity:

$$F_v = -\rho_{air} K_C \frac{\partial \bar{C}}{\partial z} \quad (3.7)$$

where K_C denotes turbulent exchange coefficient, $\bar{C}$ represents average CO_2 concentration, converted from measured mixing ratio at the measured T and P.

Following the turbulent mixing-length theory and the friction velocity definition $u_* = (-\overline{u'w'})^{1/2}$,

$$K = l u_* \quad (3.8)$$

$$u_* = l \frac{\partial \bar{U}}{\partial z} = \kappa z \frac{\partial \bar{U}}{\partial z} \quad (3.9)$$

where l is the mixing length and κ is the von Karman constant (κ=0.4).

https://doi.org/10.5194/egusphere-2026-561
Preprint. Discussion started: 4 February 2026

Stratification effects were incorporated using a stability correction, given by

$$l = m\kappa z \tag{3.10}$$

where m is the stratification correction parameter, determined as a function of the gradient Richardson number (R_i)

$$m = (1 - R_i)^{1/2} \tag{3.11}$$

Under neutral stratification conditions ($R_i = 0$), m = 1. For computational convenience, the gradient Richardson number R_i is approximated by the bulk Richardson number in finite-difference form

$$R_i \approx R_B = \frac{\frac{g\Delta\bar{\theta}}{\bar{\theta}\Delta z}}{\left(\frac{\Delta\bar{U}}{\Delta z}\right)^2} = \frac{g}{\bar{\theta}}\frac{\Delta\bar{\theta}\Delta z}{(\Delta\bar{U})^2} \tag{3.12}$$

where g is the gravitational acceleration constant; $\Delta\bar{\theta}$ and $\Delta\bar{U}$ represent the mean temperature change and wind speed change between the layers (Δz); $\bar{\theta}$ is the mean temperature between the layers.

Because forest canopies consist of complex underlying surfaces, wind profiles may deviate from the ideal logarithmic form. The surface-layer wind profile was therefore expressed as

$$\bar{U} = \frac{u_*}{\kappa} ln \frac{z-d}{z_0} \tag{3.13}$$

where d is the zero-plane displacement height, typically equal to 70%-80% of the vegetation height, and z_0 is the surface roughness length.

Assuming neutral atmospheric stratification and treating u_*, d, and z_0 as constants over the same time period, u_* can be derived from wind measurements at two heights thereby eliminating z_0 from Eq. (3.13) and rearranging the equation so that

$$u_* = \frac{\kappa(\overline{U_2} - \overline{U_1})}{\ln[(z_2 - d)/(z_1 - d)]} \tag{3.14}$$

where $\overline{U_1}$ and $\overline{U_2}$ are the mean horizontal wind speeds at heights z_1 and z_2, respectively. In the present study, the two mean horizontal wind speeds were taken from the horizontal wind measurements at any two heights as the UAV ascended during the vertical profile measurements. Substituting Eq. (3.10), Eq. (3.11) and Eq. (3.14) into

https://doi.org/10.5194/egusphere-2026-561
Preprint. Discussion started: 4 February 2026

Eq. (3.8) yields

$$K = \kappa^2(1-R_i)^{1/2}\frac{(\overline{U_2}-\overline{U_1})}{\ln[(z_2-d)/(z_1-d)]}(z-d) \quad (3.15)$$

Substitute Eq. (3.15) into Eq. (3.7) and integrate to obtain the vertical flux

$$F_v = \rho_{air}\kappa^2(1-R_i)^{1/2}\frac{(\overline{U_2}-\overline{U_1})(\overline{C_1}-\overline{C_2})}{\{\ln[(z_2-d)/(z_1-d)]\}^2} \quad (3.16)$$

where $\overline{C_1}$ and $\overline{C_2}$ represent the mean concentrations of CO_2 at heights z_1 and z_2, respectively, converted from measured CO_2 mixing ratios at the measured T and P at both heights during the UAV ascent.

The vertical CO_2 emission ($E_{C,VT}$) is finally expressed as

$$E_{C,VT} = A\rho_{air}\kappa^2(1-R_i)^{1/2}\frac{(\overline{U_2}-\overline{U_1})(\overline{C_1}-\overline{C_2})}{\{\ln[(z_2-d)/(z_1-d)]\}^2} \quad (3.17)$$

In summary, horizontal CO_2 emission components were derived from box-pattern measurements using the divergence theorem, whereas vertical emission components were obtained from profile-pattern measurements using the gradient method. The reliability of the vertical flux estimates, computed using Eq (3.18), was evaluated through direct comparisons with results from EC tower observations (see Section 4.2.1).

3.3 EC system data processing

The EC system consisted of a three-dimensional ultrasonic anemometer (CSAT3, Campbell Scientific, USA), an open-path CO_2/H_2O analyzer (LI-7500, LI-COR Biosciences, USA), and a datalogger (CR3000, Campbell Scientific, USA). Raw data were acquired at a sampling frequency of 10 Hz. The time lag between wind and gas measurements was corrected following the method of Sahlée et al. (2007). Standard quality-control procedures were applied to the turbulence data (*SI Appendix*, S1).

Fluxes were computed over 30 min averaging intervals, and coordinate rotation, virtual temperature correction, and frequency-response correction were applied to ensure high-quality vertical flux estimates. The friction velocity (u_*) and scalar fluxes (F_v) were computed as

$$u_* = (-\overline{u'w'})^{1/2} \quad (3.18)$$

$$F_v = \rho_{air}\overline{w'c'} \quad (3.19)$$

where the primes denote turbulent fluctuations of the corresponding variables.

https://doi.org/10.5194/egusphere-2026-561
Preprint. Discussion started: 4 February 2026

4 Results and discussion

4.1 Gas analyzer comparison test

To evaluate the consistency between different CO_2 analyzers, ground-based intercomparison experiments were conducted using an open-path eddy covariance analyzer (LI-7500) and the closed-path analyzer (MIRA) used on the UAV. The experiment was performed from 21:00 to 22:00 local time on 12 August 2024 (Fig. 4). The air inlets of the two analyzers were positioned at the same height to ensure sampling of the same air mass, with the LI-7500 operating at 10 Hz and the MIRA analyzer at 1 Hz. The MIRA analyzer operates in the mid-infrared (MIR) spectral range, where CO_2 absorption is substantially stronger than in the near-infrared, enabling a high sensitivity within a compact optical cell. A fixed time lag of 5 s, associated with air flow through the sampling line, was applied to synchronize the MIRA measurements with the LI-7500 data.

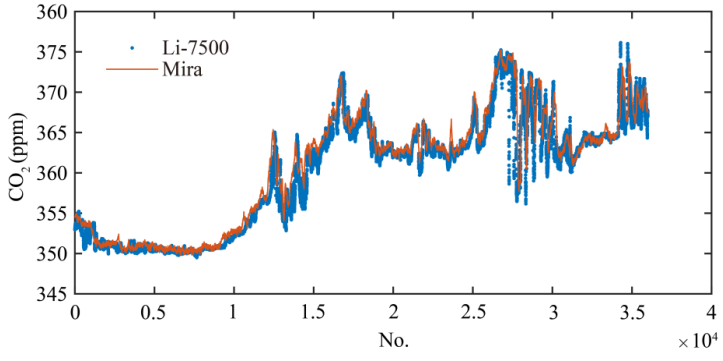

Figure 4. The comparative chart of CO_2 mixing ratio measured by the LI-7500 and Mira.

As shown in Fig. 4, the CO_2 mixing ratios measured by the two instruments exhibit highly consistent temporal variabilities, although small differences in absolute values and short-term fluctuations are present. Both datasets show a pronounced increase in

https://doi.org/10.5194/egusphere-2026-561
Preprint. Discussion started: 4 February 2026

CO_2 mixing ratio during the initial phase of the experiment, followed by enhanced variability with multiple peaks, and sustained elevated concentrations during the later period. The overall temporal coherence between the two datasets is strong, indicating that both instruments capture the same underlying CO_2 fluctuation dynamics. The MIRA measurements tend to report slightly lower CO_2 mixing ratios than the LI-7500. This attenuation is primarily attributed to high-frequency losses associated with the closed-path sampling system, including viscous damping within the tubing, interactions with the sampling line material, and signal smoothing induced by the sampling line. Such attenuation is a well-documented characteristic of closed-path systems and does not compromise the ability of the analyzer to resolve mean concentration levels and mesoscale variability. In summary, despite minor attenuations at high frequencies, the closed-path MIRA analyzer demonstrates a strong agreement with the EC-based LI-7500 measurements, supporting its suitability for CO_2 measurements from the UAV-based platform.

4.2 In-flight comparison test

4.2.1 Seasonal variability of vertical fluxes

A key part of the present study is to determine reliable vertical flux measurements using the UAV platform over a forest ecosystem on complex terrains. To quantitatively evaluate the agreement between UAV-based profile retrievals and EC tower measurements, the UAV-derived vertical CO_2 flux (F_v) and friction velocity (u_*) against their EC counterparts (Fig. 5). Because both datasets contain measurement uncertainties, the Reduced Major Axis (RMA) regression (Smith, 2009; Warton et al., 2006), which is more appropriate than ordinary least squares when neither datasets can be treated as error-free. The season-specific RMA slope, intercept, and coefficient of determination (R^2) are summarized in Table 3.

https://doi.org/10.5194/egusphere-2026-561
Preprint. Discussion started: 4 February 2026

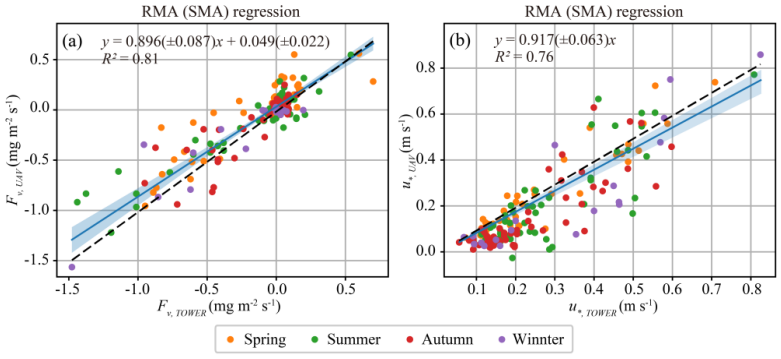

Figure 5. Reduced major axis (RMA/SMA) regressions comparing UAV-based measurements with EC tower observations across all seasons. Panel (a) shows CO_2 flux (F_c) and panel (b) shows friction velocity (u_*). Points are colored by season (Spring, Summer, Autumn, Winter). The solid blue line denotes the RMA fit, the shaded band indicates the 95% confidence interval (CI) of the regression line, and the dashed black line represents the 1:1 reference. Regression equations (slope ± 95% CI and intercept ± 95% CI) and R^2 are reported in each panel.

Table 3. Seasonal reduced major axis (RMA/SMA) regression results comparing UAV-derived measurements with EC tower observations for CO_2 flux (F_v) and friction velocity (u_*). For each season (spring, summer, autumn, winter), the table reports the sample size (n), coefficient of determination (r^2), RMA slope and its 95% confidence interval (CI), and the intercept of the relationship $y_{\mathrm{UAV}} = \mathrm{slope}\, x_{\mathrm{TOWER}} + \mathrm{intercept}$. The u_* regressions are constrained to pass through the origin (intercept fixed at 0).

Variables	Season	n	r^2	Slope	95% CI of Slope	Intercept
F_v	Spring	40	0.792	0.928	[0.777, 1.074]	0.127
	Summer	52	0.880	0.801	[0.694, 0.929]	0.034
	Autumn	55	0.744	0.997	[0.771, 1.281]	0.022
	Winter	20	0.840	0.940	[0.551, 1.079]	0.013
$u*$	Spring	40	0.888	1.012	[0.926, 1.093]	0
	Summer	52	0.714	0.915	[0.790, 1.021]	0
	Autumn	55	0.710	0.819	[0.679, 0.951]	0
	Winter	20	0.782	0.914	[0.677, 1.059]	0

As shown in Fig. 5a, UAV-derived $F_{v,UAV}$ exhibits a clear linear relationship with EC $F_{v,TOWER}$, with points generally distributed around the 1:1 line, indicating that the UAV approach captures the temporal variability of canopy-scale vertical CO_2 exchange.

https://doi.org/10.5194/egusphere-2026-561
Preprint. Discussion started: 4 February 2026

Table 3 further demonstrates consistently strong coefficients of determination across seasons (R^2=0.744-0.880). The slope, slightly lower than unity, suggests a modest "range compression" in the UAV-derived fluxes, meaning that the magnitudes tend to be slightly attenuated under strong emission or strong uptake conditions (large positive/negative fluxes). In spring, the slope is 0.928 (95% CI: [0.777, 1.074], R^2=0.792), and in autumn the slope is 0.997 (95% CI: [0.771, 1.281], R^2=0.744); both are close to unity and their confidence intervals encompass 1, suggesting good consistency in flux magnitude. In summer, the slope decreases to 0.801 (95% CI: [0.694, 0.929], R^2=0.880), and the confidence interval does not include 1, indicating a smaller flux magnitude during periods of stronger exchange. Hence the slightly lower $F_{v,UAV}$ than $F_{v,Tower}$ likely reflects enhanced nonstationarity and rapid scalar fluctuations during peak growing season, which increase sensitivity to sampling height from ground and platform-related perturbations. In winter, the slope is 0.940 (95% CI: [0.551, 1.079], R^2=0.840), showing strong correlation but larger uncertainty due to the smaller sample size (n=20).

Figure 5b shows a clear linear relationship between friction velocity $u_{*,UAV}$ and $u_{*,TOWER}$. Because u_* should physically approach zero under very weak turbulence, an origin-constrained regression (intercept fixed at 0) was used to avoid non-physical extrapolation from a free intercept. The full-sample RMA regression is:

$$u_{*,UAV}=0.917(\pm0.063)u_{*,TOWER},\ R^2=0.76 \quad (4.1)$$

This result indicates that the UAV platform captures the variations in turbulent intensity well (R^2 ≈0.76), while the slope below unity suggests a slight multiplicative underestimation of u_* relative to tower observations. Regressions for different seasons (Table 3) further indicate that the best agreement occurs in spring, with a slope of 1.012 (95% CI: [0.926, 1.093], R^2 =0.888). In contrast, $u_{*,UAV}$ shows a slight underestimation relative to $u_{*,TOWER}$ in summer, autumn, and winter, respectively, with a slope of 0.915, 0.819, 0.914.

Taken together, Fig. 5 and Table 3 demonstrate that the UAV platform reproduces the tower-observed variability of both canopy-scale CO_2 exchange and key turbulence

https://doi.org/10.5194/egusphere-2026-561
Preprint. Discussion started: 4 February 2026

metrics across all seasons (R^2=0.81 for F_v and R^2=0.76 for u_*), supporting the feasibility and robustness of such UAV profile measurements for monitoring above-canopy exchange. Nevertheless, two systematic features warrant attention: (i) F_v magnitudes tend to be slightly underestimated in summer (slope significantly < 1), and (ii) u_* shows a slight overall underestimation under the origin-constrained regression.

4.2.2 Diurnal variability of vertical fluxes

To further evaluate the applicability and consistency of the UAV-based profiling method under different diurnal conditions, the UAV-derived F_v estimates were grouped and compared with results from EC observations in three time periods: early morning (06:00–08:00 LST), noon (13:00–15:00 LST), and evening (19:00–21:00 LST). Reduced Major Axis (RMA/SMA) regression was applied to both the vertical CO_2 flux (F_v) and the friction velocity (u^*) for each time period (Fig. 6), with the corresponding statistical results summarized in Table 4.

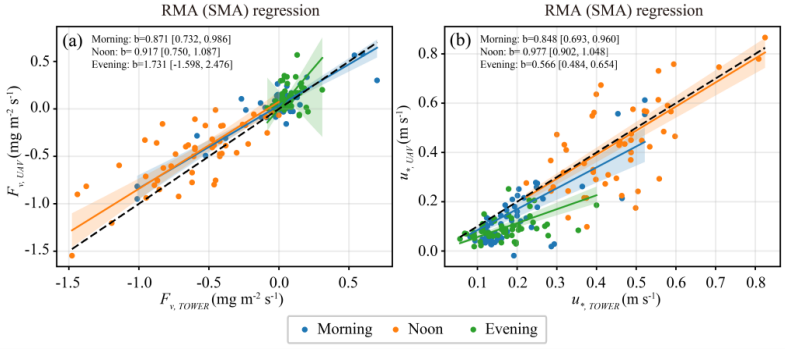

Figure 6. Reduced major axis (RMA/SMA) regressions comparing UAV-based measurements with EC tower observations for (a) CO_2 flux (F_v) and (b) friction velocity (u_*) grouped by time of day. Data are separated into morning (06:00–08:00 LST), noon (13:00–15:00 LST), and evening (19:00–21:00 LST) and shown with different colors. Solid colored lines represent the RMA fits for each time period, and the shaded bands indicate the 95% confidence intervals. The dashed black line denotes the 1:1 reference. Reported in each panel are the RMA slopes and their 95% confidence intervals; the u_* regressions in panel (b) are constrained to pass through the origin (intercept fixed at 0).

As shown in Table 4, the RMA regressions for F_v exhibit relatively strong

https://doi.org/10.5194/egusphere-2026-561
Preprint. Discussion started: 4 February 2026

correlations during the early morning and midday periods (R^2=0.806, n=63 and R^2=0.752, n=550, respectively). The corresponding slopes are 0.871 (95% CI: [0.732, 0.986]) for early morning and 0.916 (95% CI: [0.750, 1.087]) for midday, both close to unity but slightly lower than 1, indicating a modest amplitude compression. This suggests that the UAV-based method is generally capable of reproducing the variability of CO_2 fluxes observed by the EC system, while tending to underestimate flux magnitudes under stronger exchange conditions. This behavior is consistent with the seasonal-scale results presented in Section 4.2.1 and likely reflects the increased sensitivity of the gradient method to strong flux events under limited vertical sampling resolution and short-term nonstationary conditions.

Table 4. Reduced major axis (RMA/SMA) regression statistics for comparisons between UAV-based measurements and EC tower observations, grouped by time of day (morning, noon, and evening). Results are reported for CO_2 flux (F_v) and friction velocity (u_*), including sample size (n), coefficient of determination (r^2), RMA slope, the 95% confidence interval (CI) of the slope, and the intercept for the relationship $y_{\mathrm{UAV}} = \text{slope}\ x_{\mathrm{TOWER}} + \text{intercept}$. For u_*, the regression is constrained to pass through the origin (intercept fixed at 0).

Variables	Period	n	r^2	Slope	Slope of 95% CI	Intercept
F_v	Moring	63	0.806	0.871	[0.732, 0.986]	0.034
	Noon	50	0.752	0.916	[0.750, 1.087]	0.075
	Evening	54	0.055	1.730	[-1.598, 2.476]	0.002
$u*$	Moring	63	0.786	0.848	[0.926, 1.093]	0
	Noon	50	0.748	0.977	[0.790, 1.021]	0
	Evening	54	0.180	0.566	[0.679, 0.951]	0

In contrast, the agreement for F_v deteriorates substantially during the evening period, with a low coefficient of determination (R^2=0.055, n=54) and a highly uncertain slope (1.730, with a 95% confidence interval spanning both positive and negative values). The primary reason for such a comparison result is that low nighttime turbulence leads to vertical fluxes, for which the UAV methodology produces large uncertainties in the derived vertical fluxes with an apparent low bias in the estimates

https://doi.org/10.5194/egusphere-2026-561
Preprint. Discussion started: 4 February 2026

compared to EC measurements. It should be noted, however, that EC vertical flux measurements under such low turbulence conditions also bear large uncertainties, and hence this comparison only implies a low bias in the UAV methodology relative to the EC methodology, and does not indicate the absolute errors in the UAV-determined F_v. In the late afternoon to evening, as radiative forcing weakens and a stable stratification develops, turbulence above the canopy diminishes, leading to much reduced vertical fluxes. Consequently, the relative contributions of flux source–sink terms, storage, and horizontal transport—particularly advection and non-stationary transport under weak-wind conditions—increase, rendering the stationarity and horizontal homogeneity assumptions of the eddy covariance (EC) method more susceptible to violation. Aubinet et al. (2002) and Gu et al. (2005) also reported that under low-turbulence nighttime conditions, the EC method substantially underestimates ecosystem respiration fluxes.

Figure 7 presents the seasonal distributions of nighttime CO_2 flux differences, defined as $\Delta F_v = F_{v,UAV} - F_{v,Tower}$, for spring, summer, autumn, and winter. Overall, the distributions of nighttime ΔF_v show similar central tendencies across the four seasons. The mean values are small, with absolute values generally smaller than 0.1, indicating that the nighttime CO_2 flux differences between UAV-based estimates and EC tower measurements are small in magnitude for all seasons. The one-way analysis of variance (ANOVA) further confirms that the seasonal differences in nighttime ΔF_v are not statistically significant. In the analysis, F=2.50, which represents the variability among seasons, is approximately 2.50 times larger than the random variability within seasons; p =0.0699 > 0.05, representing the differences among seasons, is not statistically significant. These ANOVA results are consistent with the distribution patterns illustrated in the boxplots, which show no evident systematic seasonal shifts in nighttime flux differences.

https://doi.org/10.5194/egusphere-2026-561
Preprint. Discussion started: 4 February 2026

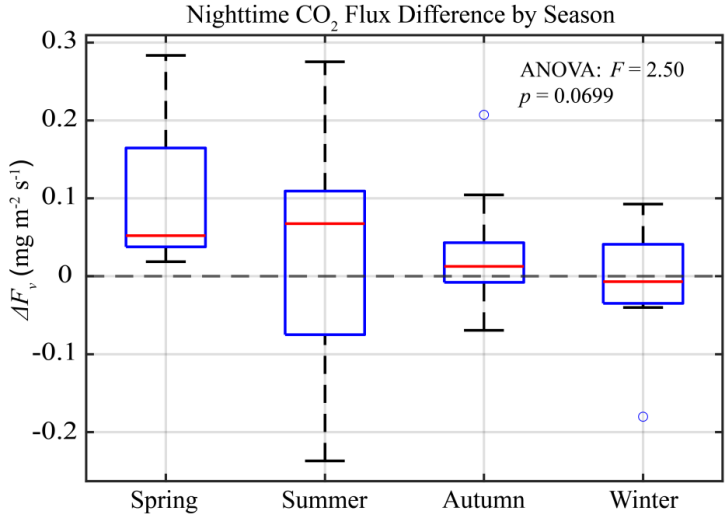

Figure 7. Boxplots of nighttime differences in CO_2 fluxes (ΔF_c) between UAV and EC tower observations across four seasons. The boxes indicate the interquartile range with median values shown as horizontal lines, small circles represent outliers and whiskers represent 1.5 times the interquartile range.

Overall, the nighttime ANOVA analysis further confirms, from a statistical perspective, the consistency between UAV-based and EC tower vertical flux observations at the seasonal scale. When combined with the results obtained from the RMA regression analysis presented above, it can be seen that although flux measurements under nighttime conditions are associated with relatively higher uncertainties, the overall differences between UAV-derived and tower-based observations remain small and do not exhibit pronounced seasonal shifts. This indicates that, despite the apparent low bias using the RMA regression analysis under weak nighttime turbulence conditions, CO_2 fluxes derived from the UAV platform are not statistically different from those derived from tower-based measurements.

Figure 8 illustrates the seasonal and diurnal variability of the UAV-derived vertical CO_2 fluxes across morning, noon, and evening periods for all four seasons. Distinct diurnal patterns are evident in every season. Midday periods consistently exhibit the strongest downward CO_2 fluxes, corresponding to maximum ecosystem uptake, particularly in spring, summer, and autumn. In contrast, morning and evening fluxes

https://doi.org/10.5194/egusphere-2026-561
Preprint. Discussion started: 4 February 2026

remain close to neutral or weakly positive, reflecting reduced turbulent mixing and lower photosynthetic activity. This diurnal structure aligns with the canonical coupling between solar radiation, canopy photosynthesis, and boundary-layer turbulence.

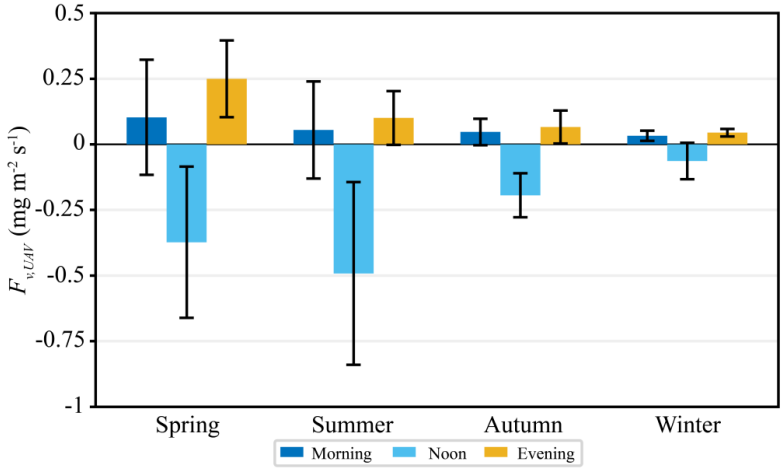

Figure 8. Seasonal variations of UAV-derived vertical CO_2 fluxes during morning, noon, and evening across spring, summer, autumn, and winter. Bars represent the mean flux for each period, and error bars indicate one standard deviation. Positive values denote upward (emission) fluxes, while negative values represent downward (uptake) fluxes.

Seasonal contrasts are equally pronounced. Summer and spring display the strongest net CO_2 uptake, consistent with high leaf area index, favorable moisture conditions, and strong radiative forcing in this subtropical forest. Autumn fluxes are weaker, reflecting declining physiological activity, while winter fluxes cluster near zero, with negligible uptake or slight emissions across all periods. The ordering of seasonal uptake strength - summer > spring > autumn ≫ winter - is consistent with long-term EC observations at this site (Yu et al., 2008).

The observed diurnal and seasonal structures in the UAV-based vertical fluxes closely match those reported in previous tower-based studies at the Qianyanzhou station (Yu et al., 2006; Zhang et al., 2014) and in other temperate and subtropical forest ecosystems (Baldocchi, 2008; Goulden et al., 1996). These results therefore not only summarize the observed variability but also provide an ecologically meaningful

https://doi.org/10.5194/egusphere-2026-561
Preprint. Discussion started: 4 February 2026

consistency check for the UAV-based vertical flux approach.

4.3 Spatial heterogeneity of net CO_2 emission

To verify whether net emissions (E_C) calculated using the mass-balance approach differ across spatial scales, emission computations were made for three box-shaped control volumes constructed from the UAV flight tracks with different horizontal scales (50×50, 100×100, and 150×150 m; height=50 m). The vertical contribution term $E_{C,VT}$ and the horizontal transport contribution term $E_{C,H}$ within each control volume were separately computed as per the detailed outlines above. Net emission is defined as $E_C = E_{C,VT} + E_{C,H}$, with uncertainties estimated at 15% (see Section 4.4 for details). To remove effects arising from differences in areas covered by the boxes, the net emissions were normalized by the areas of the boxes to give area-normalized emission intensity $e_C = E_C/A$, where A denotes the bottom area of the box. To minimize the influence of different time periods and seasons on the statistics, and according to the analysis in Section 4.2, the UAV measurements collected in summer morning and noon, which show better agreement with the EC tower comparisons, were selected for the spatial heterogeneity analysis.

If the CO_2 source-sink distribution in this region were spatially uniform, then by mass conservation the area-normalized emission intensity would be equal, i.e., $e_C(150) \approx e_C(100) \approx e_C(50)$ would be true. Based on the mean annotations of three box scales in Fig. 9 are -0.25, -0.30, and -0.24 (units: mg m^{-2} s^{-1}). This indicates a pronounced net CO_2 uptake (i.e., negative emissions) of the system as a whole at summer noon, while the differences among spatial scales are clearly smaller than the 15% systematic uncertainty. This result may suggest relatively weak spatial heterogeneity during the summer-noon period. Furthermore, one-way ANOVA shows the mean differences in e_C among the three scales were not significant (F=0.349, p=0.710). Overall, under summer-noon conditions, the area-normalized net exchange intensity is insensitive to the horizontal scales examined, and within-group variability dominates (Fig. 9).

In addition, the median values of $E_{C,H}/E_{C,VT}$ in Table 5 are very small (≈0.5%–2.4%), indicating that the system at summer noon is primarily vertical-exchange

https://doi.org/10.5194/egusphere-2026-561
Preprint. Discussion started: 4 February 2026

dominated with horizontal transport being nearly negligible. This pattern is readily explained: under summer-noon conditions, when turbulent mixing is stronger and horizontal concentration gradients are comparatively weak, the net budget (E_C) of the control volume is governed mainly by vertical turbulent exchange ($E_{C,VT}$), whereas horizontal transport ($E_{C,H}$) contributes only a minor fraction. The negative sign of the ratio suggests that the horizontal and vertical terms often have opposite signs (e.g., the vertical term indicates uptake and is negative, while the horizontal term may represent a weak compensating inflow/outflow, yielding a small positive or negative contribution), but its magnitude remains far smaller than that of the vertical term.

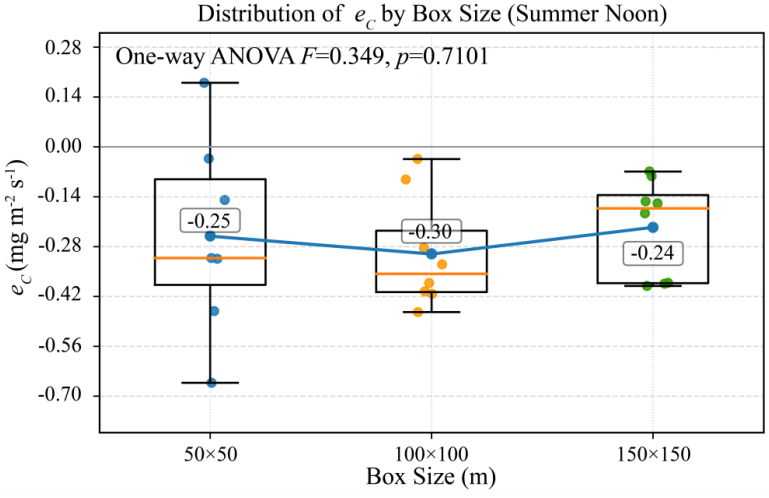

Figure 9. Distribution of e_C across box sizes (50×50 m, 100×100 m, 150×150 m) of summer noon. Boxes represent the interquartile range (*IQR*), the center line is the median, and whiskers extend to 1.5×*IQR*. Colored points are individual samples. The blue solid polyline connects the mean e_C of each group, with boxed numerical annotations.

Table 5. Summary statistics of net CO_2 emission estimates (E_C) derived from three box sizes during summer noon and autumn morning. For each box size, n denotes the number of valid samples. Reported metrics include the mean and median of E_C (kg h^{-1}), the interquartile range (*IQR*), and the median ratio $E_{C,H}/E_{C,V}$, where $E_{C,H}$ and $E_{C,V}$ represent the horizontal-transport and vertical-exchange contributions to the net emission, respectively.

	Box Size (m)	n	E_C Mean (kg h^{-1})	E_C Median (kg h^{-1})	*IQR* (kg h^{-1})	Median $E_{C,H}/E_{C,VT}$
Summer Noon	50×50	7	-2.235	-2.787	2.648	-0.024
	100×100	8	-10.732	-12.722	6.149	-0.005

https://doi.org/10.5194/egusphere-2026-561
Preprint. Discussion started: 4 February 2026

	150×150	8	-18.148	-13.889	19.859	-0.019
Autumn Morning	50×50	7	0.166	0.138	1.849	3.214
	100×100	8	7.720	7.292	2.875	0.847
	150×150	8	9.278	11.950	14.92	1.213

Another case study of spatial heterogeneity is based on the autumn-morning dataset (Fig.10). The mean values in Fig.10 indicate that the emission intensities (e_C) derived for different box sizes (0.02, 0.21, and 0.11, respectively) differ to some extent. The differences among box sizes are substantially larger than the uncertainty of the method used in this study (15%), representing e_C differ of various sizes. One-way ANOVA analysis also shows the differences in e_C among the three scales were significant (F=4.482, p=0.025). This providing direct evidence that the vegetation–atmosphere CO_2 source-sink distribution in the upper layer is spatially heterogeneous.

In addition, the component-wise contribution analysis (Table 5) indicates that the relative contribution of the horizontal transport term is markedly enhanced. The median metric, median $E_{C,H}/E_{C,VT}$, is 3.214 for 50×50, 0.847 for 100×100, and 1.213 for 150×150. These results suggest that there is a significant spatial heterogeneity in the CO_2 emissions/uptake in the range covered by the different boxes leading to horizontal CO_2 concentration gradients, and as a result near-surface horizontal CO_2 gradients under the measured horizontal winds are non-negligible within small control volumes. As the control-volume scale increases, local "hotspots/coldspots" and horizontal gradient structures are spatially averaged, weakening the relative influence of $E_{C,H}$ and thereby causing E_C to exhibit scale sensitivity.

This scale sensitivity further highlights the true advantage of UAV observations for characterizing spatial heterogeneity. UAV measurements can provide multipoint, three-dimensional CO_2 distributions and associated wind speed gradient information within a short time window, enabling the simultaneous estimation of $E_{C,H}$ (horizontal transport) and $E_{C,V}$ (vertical transport) within a consistent data framework. Moreover, by varying the box sizes, the same dataset can be re-aggregated into different spatial scales to facilitate a multi-scale comparison. In contrast, flux towers (eddy covariance)

https://doi.org/10.5194/egusphere-2026-561
Preprint. Discussion started: 4 February 2026

essentially measure point-based vertical turbulent fluxes, whose representativeness is determined by a footprint that varies with wind direction and atmospheric stability. As a result, EC tower observations yield a footprint-weighted effective flux, making it difficult to construct a spatial control volume and impossible to explicitly resolve the lateral transport term $E_{C,H}$. Therefore, box-size dependence driven by spatial heterogeneity is more readily captured by UAV observations, whereas EC towers are limited in both observation geometry and the types of physical quantities they can diagnose.

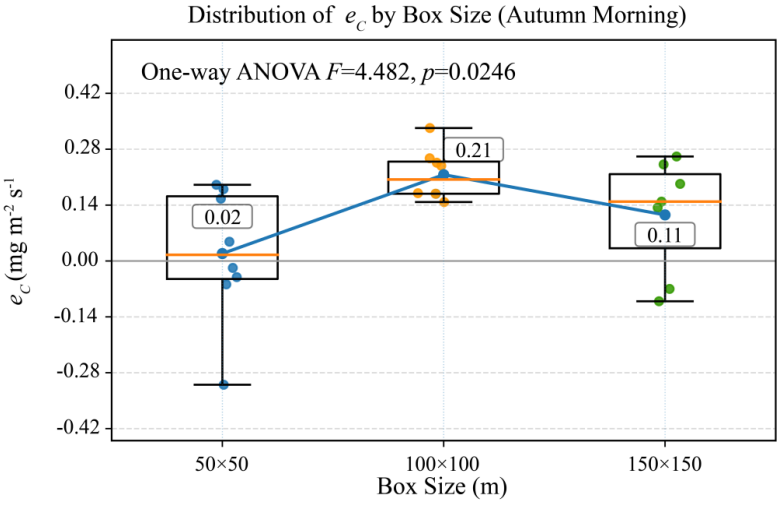

Figure 10. Distribution of e_C across box sizes (50×50 m, 100×100 m, 150×150 m) of autumn morning. Boxes represent the interquartile range (*IQR*), the center line is the median, and whiskers extend to 1.5×*IQR*. Colored points are individual samples. The blue solid polyline connects the mean e_C of each group, with boxed numerical annotations.

4.4 Computation of uncertainties

The uncertainty of the final CO_2 emission estimates was quantified by considering three independent sources: instrumental errors (δ_M), wind-calibration uncertainty (δ_V), and thermodynamic variability associated with temperature and pressure (δ_{dens}). These contributions were combined in quadrature:

$$\delta^2 = \delta_M^2 + \delta_V^2 + \delta_{dens}^2 \quad (4.7)$$

https://doi.org/10.5194/egusphere-2026-561
Preprint. Discussion started: 4 February 2026

Table 6 presents all uncertainties of the CO_2 emissions calculated for the morning, noon, and evening periods on selected days in four seasons.

Table 6. Relative uncertainties (%) of CO_2 emissions derived from the UAV for four representative days in different seasons (Spring: 12 May 2024, Summer: 20 August 2023, Autumn: 3 December 2024, and Winter: 26 December 2024). Columns labeled M, N, and E correspond to morning, noon, and evening periods, respectively. The total relative uncertainty δ is obtained by combining the individual contributions in quadrature for each period.

	12 May 2024			20 August 2023			3 December 2024			26 December 2024		
	M	N	E	M	N	E	M	N	E	M	N	E
δ_M	1	2	1	1	4	2	1	2	4	2	5	1
δ_V	6	21	13	8	11	3	5	13	8	9	2	4
δ_{dens}	0	1	0	2	1	0	0	2	0	0	1	0
δ	6	21	13	8	12	4	5	13	9	9	5	4

4.4.1 Instrumental errors

Instrumental errors are comparatively small. The ultrasonic anemometer used on the UAV has a wind speed accuracy of ±0.2 m s^{-1} and a wind direction accuracy of ±1°. For typical flight-level wind speeds of 4-6 m s^{-1}, this corresponds to a relative error of about 5% in the horizontal wind components. The closed-path CO_2 analyzer has a precision of better than 0.2 ppm, whereas the plume enhancements resolved in the box walls frequently exceed tens of ppm (e.g. up to ~40 ppm in the morning box on 8 August; Fig. 11), implying a relative CO_2 uncertainty of approximately 0.5%. Propagating these errors through the flux equations leads to an instrumental contribution to the emission rate uncertainty on the order of $\delta_M \approx 5\%$, which may be regarded as a minor term compared to sampling and methodological effects.

4.4.2 Wind-calibration uncertainties

The wind correction algorithm for platform-induced flow distortions and UAV attitude changes introduces an additional source of uncertainty. Our wind-correction algorithm, derived from extensive CFD simulations and in-flight validation (Yang et al., 2025), corrects for rotor downwash, UAV attitude changes, and background wind over a wide flight envelope conditions. Residual biases are most likely during periods of

https://doi.org/10.5194/egusphere-2026-561
Preprint. Discussion started: 4 February 2026

strong turbulence or rapid maneuvers, but the close agreement between UAV-derived friction velocity and EC-tower estimates (Fig. 5b) suggests that any remaining systematic error in wind speed is modest. The uncertainty due to the wind correction algorithm for the E_c term is estimated at 0.025 kg h^{-1} (2.1 % of E_c, minimal impact) for the 12 May 2024 flight and 0.643 kg h^{-1} (13.8 %, maximum impact) for the 3 December 2024 flight. A conservative δ_V ≈5-14% is assigned to this uncertainty term.

4.4.3 Temperature and pressure impacts

The horizontal emission term in Eq. (3.4) depends explicitly on air density, which depends on air temperature and pressure, and we use the time-averaged temperature and pressure over the duration of a box–profile pair to derive a single representative air density for the entire control volume. To assess the impact of temporal variability in thermodynamic conditions, the emission calculations were repeated using the minimum and maximum densities observed during each flight period as alternative scenarios. Table 4 shows that the uncertainties arising from variations in air density and temperature are very small (δ_{dens} ≈1-2%) and can be considered negligible.

4.4.4 Total estimated uncertainties

By combining the uncertainties from the three independent components - instrumental errors (δ_M), wind-calibration uncertainties (δ_V), and thermodynamic (temperature–pressure) variability (δ_{dens}) - the total relative uncertainty of the UAV-derived CO_2 emission rates can be obtained through quadrature addition. As shown in Table 6, the total uncertainty typically falls within 5-15%, with the exact magnitude depending on atmospheric stability, time of day, and season.

4.5 UAV measurement results

Figure 11 provides a three-dimensional visualization of the CO_2 enhancement field (ΔCO_2) measured along the walls of the 100×100 m control volume during the morning flight on 8 August 2024. The reconstructed ΔCO_2 distribution exhibits pronounced

https://doi.org/10.5194/egusphere-2026-561
Preprint. Discussion started: 4 February 2026

spatial heterogeneity, with localized high-concentration patches embedded within relatively low-background regions. In particular, a distinct hotspot reaching ~40 ppm is observed near the upper-right sector of the box, while elevated ΔCO_2 values also form elongated bands along portions of the lateral walls. This non-uniform pattern indicates that the near-canopy CO_2 field was far from horizontally homogeneous during the sampling window, consistent with the expectation of enhanced stratification and limited mixing in early morning conditions.

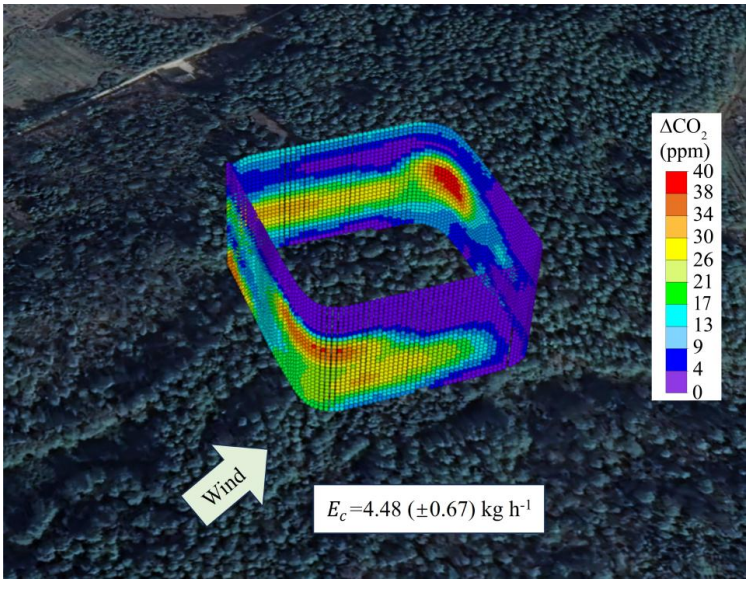

Figure 11. Three-dimensional CO_2 concentration distribution measured by the UAV (100×100 m) during the morning measurement on 8 August 2024.

The wind vector shown in Figure 11 indicates a prevailing southwesterly flow. The spatial alignment of the ΔCO_2 enhancements with the box boundaries suggests that lateral advection and flux divergence played a central role in shaping the observed concentration gradients: CO_2-enriched air masses are transported into the control volume on the upwind side and redistributed along the walls, producing strong cross-boundary gradients that dominate the mass balance. Consistent with this interpretation, the box-mass balance calculation yields a positive net exchange rate of E_c =4.48±0.67

https://doi.org/10.5194/egusphere-2026-561
Preprint. Discussion started: 4 February 2026

kg h^{-1} for the 100×100 m control volume. Breaking down the individual mass balance terms indicates that the horizontal component ($E_{C,H}$ =4.22±0.63 kg h^{-1}) accounts for nearly all of the net emission in the control volume, whereas the vertical component is small ($E_{C,VT}$ =0.26±0.04 kg h^{-1}). The near-zero vertical term is also consistent with the concurrent eddy-covariance observations similarly indicating a negligible turbulent vertical CO_2 flux. Therefore, the positive E_c primarily reflects net CO_2 inflow driven by horizontal transport (i.e., lateral convergence) rather than local vertical emission from the canopy.

Overall, the three-dimensional ΔCO_2 structure shown in Figure 11 highlights that, at this moment, CO_2 exchange above the forest canopy was controlled predominantly by horizontal transport under heterogeneous concentration fields. This underscores the importance of resolving spatial gradients and lateral boundary fluxes—features that can be captured by UAV sampling but are not directly observable from a single-point flux tower measurement.

5 Conclusions

This study developed and field-evaluated a UAV-based methodology to quantify three-dimensional CO_2 transport over a forest ecosystem by explicitly resolving both vertical exchange and horizontal advection within a three-dimensionally unified mass-balance approach, making use of an integrated UAV measurement platform and a computational algorithm that evaluates both horizontal and vertical fluxes based on a specifically designed flight strategy. Extensive applications of this methodology at the Qianyanzhou subtropical plantation forest site demonstrate that the methodology can robustly determine canopy-scale CO_2 exchange. Vertical CO_2 fluxes derived from UAV vertical profiles show excellent agreement with those determined from collocated eddy covariance (EC) tower observations across seasons, indicating that the UAV-based gradient method reproduces both the magnitude and variability of vertical turbulent exchange under typical daytime conditions. The UAV-based vertical fluxes showed that the diurnal and seasonal patterns over the forest ecosystem at Qianyanzhou - strongest

https://doi.org/10.5194/egusphere-2026-561
Preprint. Discussion started: 4 February 2026

uptake around midday during the growing season and near-neutral exchange in winter – are ecologically consistent with long-term site behavior. However, vertical fluxes of UAV and EC diverge under weak turbulence during the evening stable period, highlighting increased uncertainties for both profile-based retrievals and tower-based estimates under low vertical flux conditions.

Box-pattern UAV measurements further reveal that horizontal transport can be a dominant term under certain conditions. Enhanced CO_2 concentrations on the virtual walls of the flight boxes and wind vectors show pronounced spatial heterogeneity and lateral gradients, especially in the morning, indicating that advection-driven convergence/divergence may substantially shape the local CO_2 budget, processes that cannot be directly resolved from single-tower measurements. A multi-scale analysis using different box sizes (50×50, 100×100, and 150×150 m) shows that net emission estimates can exhibit scale dependence, reflecting the spatial heterogeneity of sources/sinks and the changing relative contribution of horizontal transport with control-volume size. These results highlight the value of UAV observations for determining spatial heterogeneity in short term ecosystem carbon exchange with the atmosphere, a task unfit for single-site measurements, for diagnosing when and where the assumption of horizontal homogeneity becomes invalid, and for quantifying lateral flux contributions explicitly.

Overall, the combined box – profile UAV framework provides a flexible and spatially explicit complement to conventional EC monitoring, offering an effective pathway to bridge the observational gap between point-scale tower fluxes and larger-scale heterogeneities, particularly over heterogeneous canopies and complex terrain. In conclusion, UAV-based platforms offer a transformative opportunity for observing ecosystem-atmosphere CO_2 exchange in three dimensions. With continued methodological refinement and broader application, such systems are well positioned to become an essential component of next-generation carbon observation strategies in forest ecosystems and beyond.

https://doi.org/10.5194/egusphere-2026-561
Preprint. Discussion started: 4 February 2026

Data availability. Data are available upon request to the corresponding author upon reasonable request.

Author contributions. HS built the unmanned aerial vehicle platform, developed the corresponding emission inversion model, and carried out the data processing, and drafted the initial version of the manuscript. SML supervised the development of the inversion model and the experimental validation in the paper, and carried out a second round of revisions to the manuscript. YW provided some key data used in the paper. YY and TH provided the wind speed correction method used in the inversion model and the validation results for horizontal emissions, respectively. KC, CL, and JZ provided assistance with the field observation experiments and revisions to the manuscript. ZM and FY provided all flux tower data from the Qianyanzhou station. JG and XG provided support for unmanned aerial vehicle flights.

Competing interests. The contact author has declared that none of the authors has any competing interests.

Disclaimer. Publisher's note: Copernicus Publications remains neutral with regard to jurisdictional claims made in the text, published maps, institutional affiliations, or any other geographical representation in this paper. While Copernicus Publications makes every effort to include appropriate place names, the final responsibility lies with the authors.

Financial support. This research has been supported by the National Key Research and Development Program of China, "Research on NQI Collaborative Innovation and Generic Key Technologies and Equipment to Support the Improvement of Data Quality for Carbon Trading" (2024YFF0618500).

https://doi.org/10.5194/egusphere-2026-561
Preprint. Discussion started: 4 February 2026

References

Aubinet, M., Heinesch, B., and Longdoz, B.: Estimation of the carbon sequestration by a heterogeneous forest: night flux corrections, heterogeneity of the site and inter-annual variability, Global Change Biology, 8, 1053-1071, https://doi.org/10.1046/j.1365-2486.2002.00529.x, 2002.

Aubinet, M., Vesala, T., and Papale, D. (Eds.): Eddy Covariance: A Practical Guide to Measurement and Data Analysis, Springer, Dordrecht, 2012.

Baldocchi, D.: Breathing of the terrestrial biosphere: lessons learned from a global network of carbon dioxide flux measurement systems, Australian Journal of Botany, 56, 1-26, https://doi.org/10.1071/bt07151, 2008.

Baldocchi, D., Falge, E., Gu, L. H., Olson, R., Hollinger, D., Running, S., Anthoni, P., Bernhofer, C., Davis, K., Evans, R., Fuentes, J., Goldstein, A., Katul, G., Law, B., Lee, X. H., Malhi, Y., Meyers, T., Munger, W., Oechel, W., U, K. T. P., Pilegaard, K., Schmid, H. P., Valentini, R., Verma, S., Vesala, T., Wilson, K., and Wofsy, S.: FLUXNET: A new tool to study the temporal and spatial variability of ecosystem-scale carbon dioxide, water vapor, and energy flux densities, Bulletin of the American Meteorological Society, 82, 2415-2434, https://doi.org/10.1175/1520-0477(2001)082<2415:Fantts>2.3.Co;2, 2001.

Baldocchi, D. D.: Assessing the eddy covariance technique for evaluating carbon dioxide exchange rates of ecosystems: past, present and future, Global Change Biology, 9, 479-492, https://doi.org/10.1046/j.1365-2486.2003.00629.x, 2003.

Bolek, A., Heimann, M., and Göckede, M.: UAV-based in situ measurements of CO2 and CH4 fluxes over complex natural ecosystems, Atmospheric Measurement Techniques, 17, 5619-5636, https://doi.org/10.5194/amt-17-5619-2024, 2024.

Bonan, G. B.: Forests and climate change: Forcings, feedbacks, and the climate benefits of forests, Science, 320, 1444-1449, https://doi.org/10.1126/science.1155121, 2008.

Cambaliza, M. O. L., Shepson, P. B., Caulton, D. R., Stirm, B., Samarov, D., Gurney, K. R., Turnbull, J., Davis, K. J., Possolo, A., Karion, A., Sweeney, C., Moser, B., Hendricks, A., Lauvaux, T., Mays, K., Whetstone, J., Huang, J., Razlivanov, I., Miles, N. L., and Richardson, S. J.: Assessment of uncertainties of an aircraft-based mass balance approach for quantifying urban greenhouse gas emissions, Atmospheric Chemistry and Physics, 14, 9029-9050, https://doi.org/10.5194/acp-14-9029-2014, 2014.

Chevallier, F., Palmer, P. I., Feng, L., Boesch, H., O'Dell, C. W., and Bousquet, P.: Toward robust and consistent regional CO2 flux estimates from in situ and spaceborne measurements of atmospheric CO2, Geophysical Research Letters, 41, 1065-1070, https://doi.org/10.1002/2013gl058772, 2014.

Crisp, D., Pollock, H. R., Rosenberg, R., Chapsky, L., Lee, R. A. M., Oyafuso, F. A., Frankenberg, C., O'Dell, C. W., Bruegge, C. J., Doran, G. B., Eldering, A., Fisher, B. M., Fu, D. J., Gunson, M. R., Mandrake, L., Osterman, G. B., Schwandner, F. M., Sun, K., Taylor, T. E., Wennberg, P. O., and Wunch, D.: The on-orbit performance of the Orbiting Carbon Observatory-2 (OCO-2) instrument and its radiometrically calibrated products, Atmospheric Measurement Techniques, 10, 59-81, https://doi.org/10.5194/amt-10-59-2017, 2017.

Feigenwinter, C., Bernhofer, C., and Vogt, R.: The influence of advection on the short term CO2-budget in and above a forest canopy, Boundary-Layer Meteorology, 113, 201-224, https://doi.org/10.1023/B:BOUN.0000039372.86053.ff, 2004.

Finnigan, J. J., Clement, R., Malhi, Y., Leuning, R., and Cleugh, H. A.: A re-evaluation of long-term flux

https://doi.org/10.5194/egusphere-2026-561
Preprint. Discussion started: 4 February 2026

measurement techniques - Part I: Averaging and coordinate rotation, Boundary-Layer Meteorology, 107, 1-48, https://doi.org/10.1023/a:1021554900225, 2003.

Foken, T.: The energy balance closure problem: An overview, Ecological Applications, 18, 1351-1367, https://doi.org/10.1890/06-0922.1, 2008.

Gioli, B., Miglietta, F., De Martino, B., Hutjes, R. W. A., Dolman, H. A. J., Lindroth, A., Schumacher, M., Sanz, M. J., Manca, G., Peressotti, A., and Dumas, E. J.: Comparison between tower and aircraft-based eddy covariance fluxes in five European regions, Agricultural and Forest Meteorology, 127, 1-16, https://doi.org/10.1016/j.agrformet.2004.08.004, 2004.

Gordon, M., Li, S. M., Staebler, R., Darlington, A., Hayden, K., O'Brien, J., and Wolde, M.: Determining air pollutant emission rates based on mass balance using airborne measurement data over the Alberta oil sands operations, Atmospheric Measurement Techniques, 8, 3745-3765, https://doi.org/10.5194/amt-8-3745-2015, 2015.

Goulden, M. L., Munger, J. W., Fan, S. M., Daube, B. C., and Wofsy, S. C.: Measurements of carbon sequestration by long-term eddy covariance: Methods and a critical evaluation of accuracy, Global Change Biology, 2, 169-182, https://doi.org/10.1111/j.1365-2486.1996.tb00070.x, 1996.

Gu, L. H., Falge, E. M., Boden, T., Baldocchi, D. D., Black, T. A., Saleska, S. R., Suni, T., Verma, S. B., Vesala, T., Wofsy, S. C., and Xu, L. K.: Objective threshold determination for nighttime eddy flux filtering, Agricultural and Forest Meteorology, 128, 179-197, https://doi.org/10.1016/j.agrformet.2004.11.006, 2005.

Han, T. R., Xie, C. H., Liu, Y. Y., Yang, Y. R., Zhang, Y. H., Huang, Y. F., Gao, X. Y., Zhang, X. H., Bao, F. M., and Li, S. M.: Development of a continuous UAV-mounted air sampler and application to the quantification of CO2 and CH 4 emissions from a major coking plant, Atmospheric Measurement Techniques, 17, 677-691, https://doi.org/10.5194/amt-17-677-2024, 2024.

Huang, M., Ji, J. J., Li, K. R., Liu, Y. F., Yang, F. T., and Tao, B.: The ecosystem carbon accumulation after conversion of grasslands to pine plantations in subtropical red soil of south China, Tellus Series B-Chemical and Physical Meteorology, 59, 439-448, https://doi.org/10.1111/j.1600-0889.2007.00280.x, 2007.

IPCC: Climate Change 2021: The Physical Science Basis., Contribution of Working Group I to the Sixth Assessment Report of the IPCC., Cambridge University Press., https://doi.org/10.1017/9781009157896, 2021.

Jacob, D. J., Turner, A. J., Maasakkers, J. D., Sheng, J. X., Sun, K., Liu, X., Chance, K., Aben, I., McKeever, J., and Frankenberg, C.: Satellite observations of atmospheric methane and their value for quantifying methane emissions, Atmospheric Chemistry and Physics, 16, 14371-14396, https://doi.org/10.5194/acp-16-14371-2016, 2016.

Jung, M., Schwalm, C., Migliavacca, M., Walther, S., Camps-Valls, G., Koirala, S., Anthoni, P., Besnard, S., Bodesheim, P., Carvalhais, N., Chevallier, F., Gans, F., Goll, D. S., Haverd, V., Köhler, P., Ichii, K., Jain, A. K., Liu, J. Z., Lombardozzi, D., Nabel, J., Nelson, J. A., O'Sullivan, M., Pallandt, M., Papale, D., Peters, W., Pongratz, J., Rödenbeck, C., Sitch, S., Tramontana, G., Walker, A., Weber, U., and Reichstein, M.: Scaling carbon fluxes from eddy covariance sites to globe: synthesis and evaluation of the FLUXCOM approach, Biogeosciences, 17, 1343-1365, https://doi.org/10.5194/bg-17-1343-2020, 2020.

Kaimal, J. C. and Finnigan, J. J.: Atmospheric Boundary Layer Flows: Their Structure and Measurement, Oxford University Press, Oxford, 1994.

Khan, A., Schaefer, D., Tao, L., Miller, D. J., Sun, K., Zondlo, M. A., Harrison, W. A., Roscoe, B., and

https://doi.org/10.5194/egusphere-2026-561
Preprint. Discussion started: 4 February 2026

Lary, D. J.: Low Power Greenhouse Gas Sensors for Unmanned Aerial Vehicles, Remote Sensing, 4, 1355-1368, https://doi.org/10.3390/rs4051355, 2012.

Langelaan, J. W., Alley, N., and Neidhoefer, J.: Wind field estimation for small unmanned aerial vehicles, Journal of Guidance Control and Dynamics, 34, 1016-1030, https://doi.org/10.2514/1.52532, 2011.

Leuning, R., Cleugh, H. A., Zegelin, S. J., and Hughes, D.: Carbon and water fluxes over a temperate Eucalyptus forest and a tropical wet/dry savanna in Australia: measurements and comparison with MODIS remote sensing estimates, Agricultural and Forest Meteorology, 129, 151-173, https://doi.org/10.1016/j.agrformet.2004.12.004, 2005.

Leuning, R., Zegelin, S. J., Jones, K., Keith, H., and Hughes, D.: Measurement of horizontal and vertical advection of CO2 within a forest canopy, Agricultural and Forest Meteorology, 148, 1777-1797, https://doi.org/10.1016/j.agrformet.2008.06.006, 2008.

Mahrt, L.: Flux sampling errors for aircraft and towers, Journal of Atmospheric and Oceanic Technology, 15, 416-429, https://doi.org/10.1175/1520-0426(1998)015<0416:Fsefaa>2.0.Co;2, 1998.

Mahrt, L.: Variability and Maintenance of Turbulence in the Very Stable Boundary Layer, Boundary-Layer Meteorology, 135, 1-18, https://doi.org/10.1007/s10546-009-9463-6, 2010.

Monin, A. S. and Obukhov, A. M.: Basic laws of turbulent mixing in the surface layer of the atmosphere, Trudy Geophys. Inst. AN. SSSR, 24, 153-187, 1954.

Niedzielski, T., Skjoth, C., Werner, M., Spallek, W., Witek, M., Sawinski, T., Drzeniecka-Osiadacz, A., Korzystka-Muskala, M., Muskala, P., Modzel, P., Guzikowski, J., and Kryza, M.: Are estimates of wind characteristics based on measurements with Pitot tubes and GNSS receivers mounted on consumer-grade unmanned aerial vehicles applicable in meteorological studies?, Environmental Monitoring and Assessment, 189, https://doi.org/10.1007/s10661-017-6141-x, 2017.

Nolan, P. J., Pinto, J., González-Rocha, J., Jensen, A., Vezzi, C. N., Bailey, S. C. C., de Boer, G., Diehl, C., Laurence, R., Powers, C. W., Foroutan, H., Ross, S. D., and Schmale, D. G.: Coordinated unmanned aircraft system (UAS) and ground-based weather measurements to predict lagrangian coherent structures (LCSs), Sensors, 18, https://doi.org/10.3390/s18124448, 2018.

Palomaki, R. T., Rose, N. T., van den Bossche, M., Sherman, T. J., and De Wekker, S. F. J.: Wind estimation in the lower atmosphere using multirotor aircraft, Journal of Atmospheric and Oceanic Technology, 34, 1183-1191, https://doi.org/10.1175/jtech-d-16-0177.1, 2017.

Pan, Y. D., Birdsey, R. A., Fang, J. Y., Houghton, R., Kauppi, P. E., Kurz, W. A., Phillips, O. L., Shvidenko, A., Lewis, S. L., Canadell, J. G., Ciais, P., Jackson, R. B., Pacala, S. W., McGuire, A. D., Piao, S. L., Rautiainen, A., Sitch, S., and Hayes, D.: A Large and Persistent Carbon Sink in the World's Forests, Science, 333, 988-993, https://doi.org/10.1126/science.1201609, 2011.

Rogers, K. and Finn, A.: Three-dimensional UAV-based atmospheric tomography, Journal of Atmospheric and Oceanic Technology, 30, 336-344, https://doi.org/10.1175/jtech-d-12-00036.1, 2013.

Sahlée, E., Smedman, A.-S., Högström, U., and Rutgersson, A.: Reevaluation of the bulk exchange coefficient for humidity at sea during unstable and neutral conditions, Journal of Physical Oceanography, 38, 257-272, https://doi.org/10.1175/2007JPO3754.1, 2008.

Schimel, D., Pavlick, R., Fisher, J. B., Asner, G. P., Saatchi, S., Townsend, P., Miller, C., Frankenberg, C., Hibbard, K., and Cox, P.: Observing terrestrial ecosystems and the carbon cycle from space, Global Change Biology, 21, 1762-1776, https://doi.org/10.1111/gcb.12822, 2015.

Schmid, H. P.: Footprint modeling for vegetation atmosphere exchange studies: a review and perspective, Agricultural and Forest Meteorology, 113, 159-183, https://doi.org/10.1016/s0168-1923(02)00107-

https://doi.org/10.5194/egusphere-2026-561
Preprint. Discussion started: 4 February 2026

7, 2002.

Shimura, T., Inoue, M., Tsujimoto, H., Sasaki, K., and Iguchi, M.: Estimation of wind vector profile using a hexarotor unmanned aerial vehicle and its application to meteorological observation up to 1000 m above surface, Journal of Atmospheric and Oceanic Technology, 35, 1621-1631, https://doi.org/10.1175/jtech-d-17-0186.1, 2018.

Smith, R. J.: Use and Misuse of the Reduced Major Axis for Line-Fitting, American Journal of Physical Anthropology, 140, 476-486, https://doi.org/10.1002/ajpa.21090, 2009.

Soddell, J. R., McGuffie, K., and Holland, G. J.: Intercomparison of atmospheric soundings from the aerosonde and radiosonde, Journal of Applied Meteorology, 43, 1260-1269, https://doi.org/10.1175/1520-0450(2004)043<1260:Ioasft>2.0.Co;2, 2004.

Soltaninezhad, M., Monsorno, R., and Tondini, S.: A Review of Methods and Challenges for Wind Measurement by Small Unmanned Aerial Vehicles, Meteorological Applications, 32, https://doi.org/10.1002/met.70065, 2025.

Spiess, T., Bange, J., Buschmann, M., and Vörsmann, P.: First application of the meteorological Mini-UAV 'M2AV', Meteorologische Zeitschrift, 16, 159-169, https://doi.org/10.1127/0941-2948/2007/0195, 2007.

Stull, R. B.: An Introduction to Boundary Layer Meteorology, Kluwer Academic Publishers, Dordrecht, 1988.

Thielicke, W., Hübert, W., Müller, U., Eggert, M., and Wilhelm, P.: Towards accurate and practical drone-based wind measurements with an ultrasonic anemometer, Atmospheric Measurement Techniques, 14, 1303-1318, https://doi.org/10.5194/amt-14-1303-2021, 2021.

Vickers, D. and Mahrt, L.: Quality control and flux sampling problems for tower and aircraft data, Journal of Atmospheric and Oceanic Technology, 14, 512-526, https://doi.org/10.1175/1520-0426(1997)014<0512:QCAFSP>2.0.CO;2, 1997.

Villa, T. F., Salimi, F., Morton, K., Morawska, L., and Gonzalez, F.: Development and Validation of a UAV Based System for Air Pollution Measurements, Sensors, 16, https://doi.org/10.3390/s16122202, 2016.

Warton, D. I., Wright, I. J., Falster, D. S., and Westoby, M.: Bivariate line-fitting methods for allometry, Biological Reviews, 81, 259-291, https://doi.org/10.1017/s1464793106007007, 2006.

Wilson, K., Goldstein, A., Falge, E., Aubinet, M., Baldocchi, D., Berbigier, P., Bernhofer, C., Ceulemans, R., Dolman, H., Field, C., Grelle, A., Ibrom, A., Law, B. E., Kowalski, A., Meyers, T., Moncrieff, J., Monson, R., Oechel, W., Tenhunen, J., Valentini, R., and Verma, S.: Energy balance closure at FLUXNET sites, Agricultural and Forest Meteorology, 113, 223-243, https://doi.org/10.1016/s0168-1923(02)00109-0, 2002.

Witte, B. M., Singler, R. F., and Bailey, S. C. C.: Development of an Unmanned Aerial Vehicle for the Measurement of Turbulence in the Atmospheric Boundary Layer, Atmosphere, 8, https://doi.org/10.3390/atmos8100195, 2017.

WMO: Greenhouse Gas concentrations hit record high. Again., press release, 15 November 2023, available at: https://wmo.int/news/media-centre/greenhouse-gas-concentrations-hit-record-high-again, last access: 28 January 2026, 2023.

Yang, Y. R., Zhang, Y. H., Han, T. R., Xie, C. H., Liu, Y. Y., Huang, Y. F., Zhou, J. T., Sun, H. J., Zhao, D. L., Zhang, K., and Li, S. M.: A correction algorithm for rotor-induced airflow and flight attitude changes during three-dimensional wind speed measurements made from a rotary unoccupied aerial vehicle, Atmospheric Measurement Techniques, 18, 3035-3050, https://doi.org/10.5194/amt-18-

https://doi.org/10.5194/egusphere-2026-561
Preprint. Discussion started: 4 February 2026

3035-2025, 2025.

Yu, G. R., Wen, X. F., Sun, X. M., Tanner, B. D., Lee, X. H., and Chen, J. Y.: Overview of ChinaFLUX and evaluation of its eddy covariance measurement, Agricultural and Forest Meteorology, 137, 125-137, https://doi.org/10.1016/j.agrformet.2006.02.011, 2006.

Yu, G. R., Zhang, L. M., Sun, X. M., Fu, Y. L., Wen, X. F., Wang, Q. F., Li, S. G., Ren, C. Y., Song, X., Liu, Y. F., Han, S. J., and Yan, J. H.: Environmental controls over carbon exchange of three forest ecosystems in eastern China, Global Change Biology, 14, 2555-2571, https://doi.org/10.1111/j.1365-2486.2008.01663.x, 2008.

Zhang, S. P., Yi, X., Zheng, X. G., Chen, Z. Q., Dan, B., and Zhang, X. Z.: Global carbon assimilation system using a local ensemble Kalman filter with multiple ecosystem models, Journal of Geophysical Research-Biogeosciences, 119, 2171-2187, https://doi.org/10.1002/2014jg002792, 2014.